A novel high temperature electrical storage heater using an inorganic salt based composite phase change material

Li, Chuan; Li, Qi; Zhao, Yanqi; Jia, Yixuan; Ding, Yufeng; Jin, Yi; Weng, Likui; Ding, Yulong

DOI:
10.1002/est2.v1.6

Document Version
Publisher's PDF, also known as Version of record

Citation for published version (Harvard):
Li, C, Li, Q, Zhao, Y, Jia, Y, Ding, Y, Jin, Y, Weng, L & Ding, Y 2019, 'A novel high temperature electrical storage heater using an inorganic salt based composite phase change material', *Energy Storage Materials*, vol. 1, no. 6, e88. https://doi.org/10.1002/est2.v1.6

Received: 8 July 2019 | Revised: 13 August 2019 | Accepted: 14 August 2019

DOI: 10.1002/est2.88

ENERGY STORAGE WILEY

RESEARCH ARTICLE

A novel high temperature electrical storage heater using an inorganic salt based composite phase change material

Chuan Li[1] | Qi Li[1] | Yanqi Zhao[1] | Yixuan Jia[2] | Yufeng Ding[2] | Yi Jin[2] | Likui Weng[2] | Yulong Ding[1]

[1]Birmingham Centre for Energy Storage (BCES) & School of Chemical Engineering, University of Birmingham, Birmingham, UK

[2]Jiangsu Jinhe Energy Science & Technology Co. Ltd., Jurong, Jiangsu Province, China

Correspondence
Yulong Ding, Birmingham Centre for Energy Storage (BCES) & School of Chemical Engineering, University of Birmingham, Birmingham, UK.
Email: y.ding@bham.ac.uk

Funding information
Engineering and Physical Sciences Research Council (EPSRC), Grant/Award Numbers: EP/P004709/1, EP/P003435/1; British Council, Grant/Award Numbers: 2016-RLWK7-10243, 2018-RLWK10-10594

Abstract

We have studied a high temperature storage heater containing an inorganic salt based composite phase change material (CPCM) for electrical load shift and operation cost reduction. The storage heater consists of CPCM modules with embedded electrical elements for charging at off-peak hours and flow channels for discharging the stored heat in a controlled manner when needed. The flow channels are for heat transfer fluid (HTF, air in this work) to exchange heat with the CPCM modules and transport the heat to the heating space. A series of experiments are carried out to study the charging and discharging behavior of the storage heater. The effects of the flow channel arrangements between the CPCM modules, and the heating element arrangements inside the heater are studied. A mathematical model is also developed to investigate the performance of the storage heater with a focus on the performance comparison of the storage heater filled with the CPCM and that with the ferric oxide bricks (the conventional sensible heat storage material), and the evaluation of temperature control strategy for the CPCM based storage heater. The results show that a charge of 8 hours of the storage heater during the off-peak period is sufficient to supply heat for the whole day under the conditions of this work. The flow channel arrangements have significant influences on the storage heater performance in terms of temperature distribution of the CPCM modules and HTF outlet temperature, and the efficiencies of the charging and discharging processes. An interlaced arrangement of CPCM modules in the heater can effectively reduce the temperature swing (eg, between 21.7°C and 22.5°C over a day) and hence improve the room thermal comfort level. The results also show that the CPCM based storage heater gives a superior performance than the ferric oxide based storage heater. Given the storage volume, the power rating, and the amount of stored heat, the mass of the ferric oxide based storage heater is more than 1.6 times that of the CPCM based storage heater. Given the mass and power rating, the heat storage capacity of the CPCM based heater is nearly 68% higher than that of

the ferric oxide based storage heater. It is also found that the heat storage performance could be enhanced through a temperature control strategy with the temperature measurement located 15 mm away from the heating elements, for which the heating elements only need two start-stops over the 8-hour charging period.

KEYWORDS

composite phase change material, high temperature, inorganic salt, latent heat storage, storage heater, temperature control strategy

1 | INTRODUCTION

The inefficient utilization of traditional fossil energy related combustion for winter heating has caused serious environmental pollution in all over the world. It is reported that nearly 10% of global total ambient $PM_{2.5}$ (from both primary PM emissions and secondary PM formation) comes from residential heating stoves and boilers in which most of the emissions are from household coal burning for space heating.[1-3] Electricity, as a clean energy source especially when produced from renewables such as wind, solar, and tide energy has almost no additional emission and is environmentally friendly, has been shown to be able to replace coal burning stoves for space heating. However, the large-scale consumption of electricity presents significant challenges to the energy networks, leading to the so-called peak and off-peak periods of power grids. Significant efforts have therefore been made to meet the peak load and narrow the gap between the peak and off-peak energy demands.[2-4] One approach that could address this challenge is the use of electrical storage heaters to shift the load from the peak period to the off-peak period.[5,6] In such devices, electrical energy is converted to thermal energy and stored in the device during the off-peak period. During the peak period, the stored thermal energy is extracted by a heat transfer fluid (HTF) by both radiation and convection (natural and/or forced) using a fan installed inside the devices. Due to the electricity cost difference between the valley and peak periods, the utilization of electrical storage heaters could also offer significant economic benefits. This work concerns the design and investigation of a novel high temperature electrical storage heater containing an inorganic salt based storage medium for electrical load shift and operation cost reduction.

There are currently two practical technologies for storing thermal energy in electrical storage heaters. One uses sensible heat storage materials, such as refractory bricks, structural cements and rocks, to name but a few, and another uses phase change materials (PCMs).[5,7-10] One of the merits of the latter is that PCMs experience a phase transition by absorbing and releasing heat under an approximately isothermal process.[11-13] Due to high heat storage density of PCMs, much smaller sizes and masses are required for a given heat storage capacity than that uses a sensible storage material, and hence, a more compact structure can be achieved. Farid and Chen[14] carried out a numerical study on an underfloor electrical storage heater to evaluate the potential of utilizing PCM to enhance the floor thermal mass, and they found that the heater containing a 30 mm PCM layer with a melting temperature of 40°C was able to provide uniform heating over the peak period with charging for only 8 hours during the off-peak period. It was demonstrated that almost 7.2 MJ/m^2 per day of electricity can be shifted by using such PCM based electrical storage heater. Later, Farid and Kong[15] reported another underfloor electrical storage system with encapsulated $CaCl_2.6H_2O$ as the PCM, and their results showed that the heat storage device was able to provide the floor surface a desired temperature of 24°C throughout the peak period after the heating was stopped. Wang et al.[16] developed a high temperature electrical storage heater using an Al-Si alloy as the PCM. The alloy was encapsulated in a clay and ceramic container to resolve the leakage problem. During off-peak period, the PCM was heated by two electrical heating components. During the peak period, air was used to extract the heat of the alloy based PCM. Their results indicated that the heater was able to provide a stable heat-releasing rate and meet the thermal comfort demand. Due to the high heat storage density of PCM and low operating cost, the heater could be an economical option for domestic space heating. Recently, Wang et al.[5] performed an experimental study on a PCM based electrical storage heater using flat micro-heat pipe arrays with a paraffin wax as PCM and air as HTF. Electric power of a range of 0.2-2.04 kW was supplied to the PCM based storage heater. They found that the heater could shift electricity from peak to off-peak time effectively with charging and discharging efficiencies of 97% and 98%, respectively.

Clearly, the conventional solid-liquid PCM based electrical storage heaters require encapsulation to avoid leakage issues, which has been shown to be able to extend the lifespan of the PCMs in storage devices. However, there are other issues such as low thermal conductivity PCM, shape stabilization, corrosion, and increased cost due to the

encapsulation. These challenges largely limit their large-scale commercial and industrial utilization. Recent investigations have demonstrated that the utilization of form-stable composite phase change material (CPCM) is able to address the PCMs related problems.[17,18] A CPCM usually consists of a PCM for heat storage, a ceramic skeleton material (CSM) for shape stabilization and a thermal conductivity enhancement material (TCEM) for heat transfer enhancement. Such an approach has been shown to give an outstanding combination of thermophysical and mechanical properties.[19-23] However, little work has been found on the use of the CPCM in the design of electrical storage heaters. Lin et al.[24,25] proposed an underfloor electrical storage system containing a shape-stabilized CPCM made of paraffin (PCM) and polyethylene (CSM) with a mass ratio of 75:25. Their results showed that the electrical storage heater could provide a uniform indoor temperature while shifting over 50% of the total electricity consumption from the peak period to the off-peak period. Zhou et al.[26] numerically studied a shape-stabilized CPCM based hybrid heating system. Using the same materials to Lin et al.,[7] a direct gain passive solar house with CPCM plates as the inner linings of walls and the ceiling was built and evaluated. Their results showed that the employment of CPCM apparently enhanced the indoor thermal comfort level and nearly 12% of total electricity consumption can be saved throughout the winter period.

In the present work, a novel high temperature electrical storage heater containing an inorganic salt based CPCM is proposed and investigated. The storage heater is designed to consist of CPCM modules with embedded electrical elements for charging at off-peak hours and flow channels for discharging the stored heat in a controlled manner. The flow channels are for HTF to exchange heat with the CPCM modules and transport the heat to the heating space. A series of experiments are carried out to study the charging and discharging behavior of the storage heater. The effects of the flow channel arrangements between the CPCM modules, and the heating element arrangements inside the heater are studied. A mathematical model is also developed to investigate the performance of the storage heater with a focus on performance comparison of the storage heater filled with the CPCM modules and that with the ferric oxide bricks (the conventional sensible heat storage materials), and the evaluation of temperature control strategy for the CPCM based storage heater. The paper is organized in the following form. First, the design of electrical storage heater, and experimental methods and procedure are presented in Section 2. The experimental results including the effects of the CPCM module arrangement on the temperature distribution and thermal cycling performance as well as charging and discharging efficiency of the heater are discussed in Section 3, followed by numerical modeling description on the CPCM based storage heater in Section 4. Focuses are then on the comparison between the CPCM based heater and the conventional storage heater, and also the temperature control strategy within the heater in Section 5. Finally, concluding remarks are given in Section 6. The results presented in this work show that the new electrical storage heater containing high temperature CPCM exhibits good performance and is sufficient to provide reasonably uniform heating throughout the whole day.

2 | DESIGN OF CPCM BASED ELECTRICAL STORAGE HEATER AND EXPERIMENTAL PROCEDURE

The design of the electrical storage heater is based on a module configuration of the CPCM. Figure 1 shows schematically the CPCM modules and their arrangement within the heater. Two rectangular CPCM modules are used as shown respectively in Figure 1 (a) and (b). The width and height of the two modules are respectively ~118 and ~45 mm; whereas the length of the module (a) is ~233 mm, which is two times that of the module (b). Both the modules have a recessed horizontal rectangular channel which defines the HTF flow passages and heating elements locations. In addition, there is a cylindrical HTF flow channel across the two modules. The CPCM modules are stacked into three vertical columns inside the heater so that the HTF can flow through the modules via the cylindrical channels, absorbing or releasing heat as illustrated in Figure 1. The thermophysical properties of the CPCM are characterized for density (Dilatometer, DIL 806, TA Instruments, UK), thermal conductivity (LFA 427, NETZSCH, Germany), and phase change point, specific heat capacity and latent heat (DSC, QMS 403D, NETZSCH, Germany). Table 1 summarizes the results.

There is an important criterion that should be considered when designing the electrical storage heater the amount of the CPCM modules should be sufficient so that the heat stored during the off-peak period (~8 hours) is able to keep the indoors temperature above or close to the desired temperature of ~18°C during the rest of ~16 hours. Hence, according to the heat storage density of the CPCM given above, the total mass of CPCM required is ~50 kg, which corresponds to ~20 pieces of module (a) and ~10 pieces of module (b) in total within the heater as showed in Figure 1. The detailed structure of the electrical storage heater is illustrated in Figure 2. The enclosure had outside dimensions of ~860 mm in length, ~620 mm in height and ~200 mm in width. Five sets of U-type electrical heating elements with the diameter of ~5 mm and total power of ~2.4 kW are placed in the recessed horizontal cuboid channels which are used to heat the CPCM modules and HTF. These heating

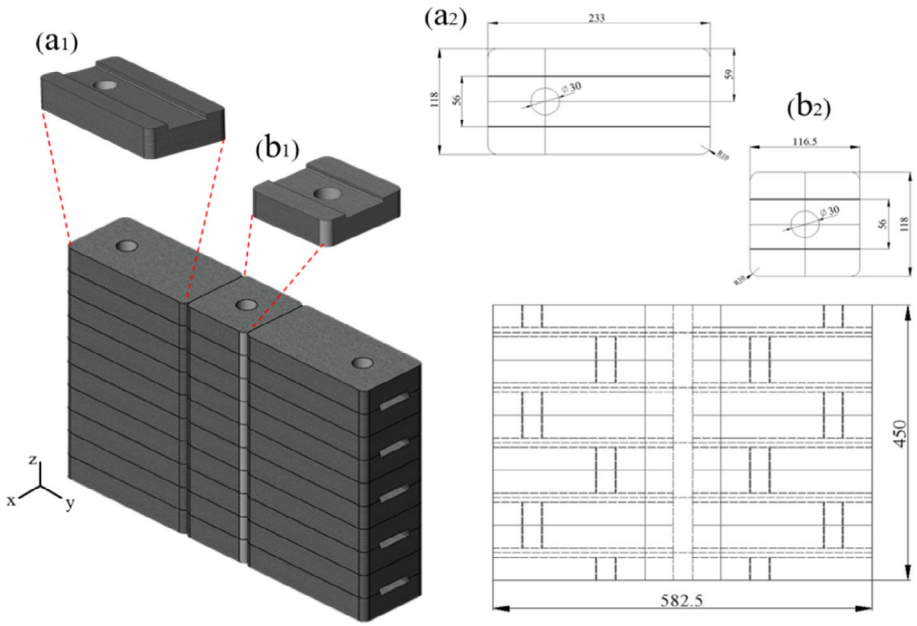

FIGURE 1 Schematic illustration of CPCM modules and their arrangement inside the heater, unit: mm

TABLE 1 Thermophysical properties of CPCM and insulating materials

Thermal-properties	Carbonate salt	Ceramic material	Graphite material	Vermiculate plate	Nano-materials plate
Density (kg/m^3)	2000	3580	1800	2400	2200
Thermal conductivity (W m^{-1} °C^{-1})	2	3	129	0.035	0.032
Heat capacity (kJ kg^{-1} °C^{-1})	1.35	0.88	0.66	1.08	0.8
Melting heat (kJ/kg)	340	-	-	-	-
Melting point (°C)	620	-	-	-	-

elements come not directly into contact with the CPCM modules and heat the modules through thermal radiation. A blower and controller are located at the left corner of the heater for controlling the convective flow of the air through the internal passages formed by the stacked CPCM modules. For reducing heat loss and ensuring safety two insulating layers, each 30 mm thick, consisting of, a vermiculate plate, and a nano-materials plate (see Figure 2). The thermophysical properties of these two insulating materials are listed in Table 1.

Figure 3 shows a schematic diagram of the experimental system that used in this work, which consists mainly of a temperature controller, the electrical storage heater and a data acquisition unit. The data acquisition unit has 10 K-type thermocouples (TC Direct, UK), a compact DAQ chassis (cDAQ-9172, National Instruments, UK), and a temperature module (NI-9211, National Instruments, UK) interfaced to a PC with a LabView programme (see Figure 3A). Eight thermocouples of T1-T8 are used to monitor the temperature of the CPCM modules which are inserted 20 mm into the modules from their sidewalls along the x-axis direction. The thermocouple T9 is for measuring the temperature of the electrical heating element. Another thermocouple (T10) is used to monitor the outlet temperature of the heater (see Figure 3B). In a typical experiment, the velocity of the air is kept at 0.01 m/s for both the charging and discharging processes. Prior to the test, the heater is warmed up until the inside average temperature reaching to around 100°C. The heater is first electrically charged for 8 hours in the evening. Then, the power is turned off automatically and the heater starts the discharging process during the day. The whole charging and discharging processes are continued for 24 hours in order to simulate the practical peak and off-peak space heating process. Note that the discharging process sustains the whole process so that the heater can meet the heating requirements not only in the peak period but also for the off-peak period. The experiments are repeated to ensure the reliability of the results.

3 | EXPERIMENTAL RESULTS AND DISCUSSION

The arrangements of the CPCM modules inside the heater affect the performance of CPCM based electrical storage

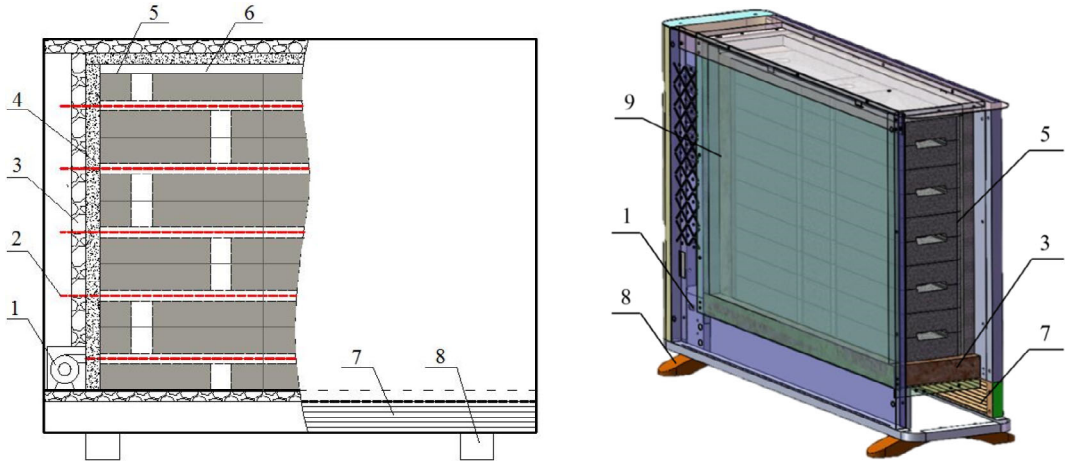

FIGURE 2 Scheme of structure of the electrical storage heater. (1) flow blower; (2) electrical heating element; (3) vermiculate insulation plate; (4) nano-materials insulation plate; (5) CPCM module; (6) air layer; (7) air outlet bail; (8) bracket; (9) shell

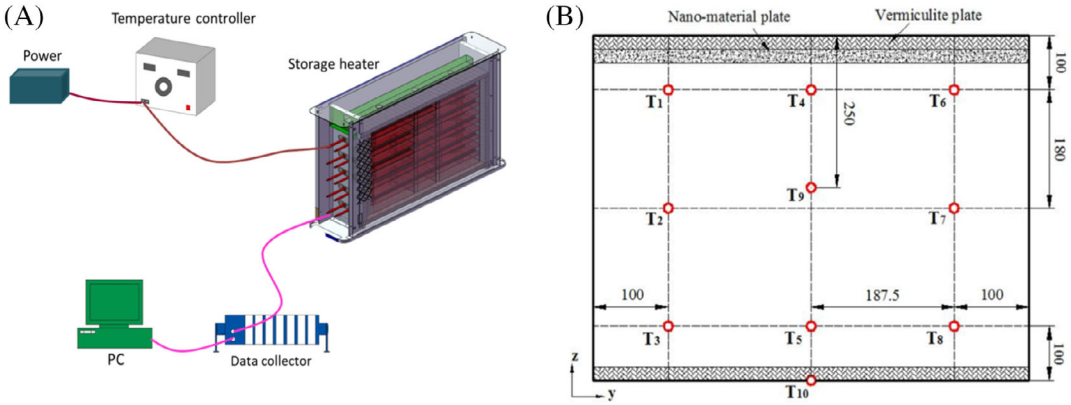

FIGURE 3 Schematic diagram of the experimental system (A) and the temperature measuring locations (B)

heater as different stacking of the CPCM modules gives a different HTF flow fields and hence different temperature distributions within the heater. As a result, the effects of different CPCM module arrangements on the thermal performance of the heater are discussed in this section. Here three cases are experimentally tested as shown in Figure 4.

3.1 | Effects of CPCM module arrangements on the temperature distributions

Figure 5 shows the temperature evolution of the CPCM modules within the heater for the three different cases both during the charging and discharging processes. In this set of studies, the power of the heating elements and the airflow rate are respectively kept at 2.4 kW and 0.01 m/s. One can see clear inhomogeneity in the temperature distributions of the CPCM modules for all three cases, demonstrating that the CPCM module arrangements presents a big effect on the temperature distribution. The measured highest temperature in the third configuration is the highest among the three cases, whereas that the first configuration gives the lowest maximum temperature, leading to the maximum temperature difference over ~150°C under this set of charging condition. Look at Figure 5A for the case 1 first, the top regions heat up faster than the bottom regions and the temperature difference of them increases with time during the charging process as the temperature rises, and tends to be lower during the discharging process. At the end of charging process, only the temperature of the modules at the top regions (point 1, point 4, and point 6) exceeds the phase change temperature of ~620°C, indicating a small portion of phase transition occurred and the heat storage inside the heater mainly in the form of sensible heat. For the second configuration, a similar temperature distribution is observed with the highest temperature in the heater appearing at the top-middle region. The left side of the heater

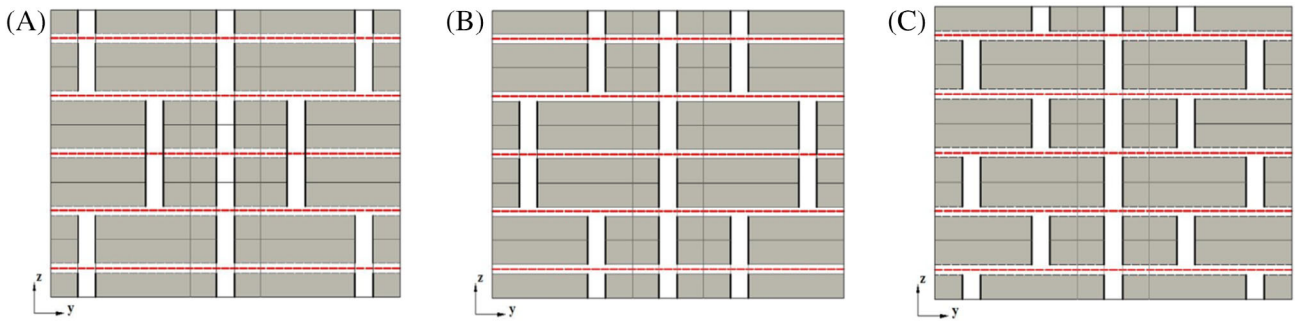

FIGURE 4 Three cases of CPCM module arrangements in the heater. (A) case 1, parallel arrangement, (B) case 2, parallel arrangement and (C) case 3, interlaced arrangement

exhibits a higher temperature than the right side, indicating a nonsymmetric temperature distribution inside the heater both during the charging and discharging processes. In the third configuration, however, it is observed that T1 and T6, and T2 and T7 all give similar readings throughout the charging period. This implies that, although the temperature is unevenly distributed, the interlaced arrangement of CPCM modules within the third configuration gives a better temperature distribution symmetry in the heater. Such an arrangement leads to the highest maximum temperature of the CPCM modules inside the heater. As shown in Figure 5C, the CPCM temperatures at all the measured points are above the melting temperature and experience the phase transition except for points 5 and 8 located at the HTF inlet, indicating that much more heat is stored during the off-peak period.

From the figure, it can also be seen that the temperature profiles of the CPCM modules at the bottom region (points 5 and 7) particularly in the second and third configurations show a clear different trend compared to other regions. During the charging process, the temperature of these bricks increases slowly and the heat is stored mainly by sensible heat, while it decreases quickly as sensible heat is released due to the forced convection during the discharging process. The above observations can be explained as follows. In the initial stage of charging, the temperature of heating elements increases rapidly and transfers the heat to the CPCM modules and the HTF through thermal radiation and forced convection, respectively. During this period, heat storage occurs mainly in the form of sensible heat. Due to the large temperature difference between the modules and the heating elements, the thermal radiation transfer is more significant than the convection and hence, dominates the heat transfer. As a result, the temperature of the modules increases much quicker than that of the HTF. With the process of the charging process, the thermal radiation transfer between the modules and the heating elements is steadily eroded as the temperature differences decreases. The HTF temperature keeps increase and starts to transfer the heat to modules. Over this period, natural convection becomes more vigorous due to hot air rising and, consequently, the maximum temperature inside the heater appears at the top region. At the HTF entrance, the cold air entering the heater keeps absorbing the heat from the bricks closed to the fan, leading to the temperature there increases slowly. This in turn gives a low temperature increase rate of the CPCM modules near the fan and hence the heat is mainly stored in the sensible form. During discharge, the power of heating elements is switched off and the heat transfer inside the heater is mainly through the forced convection. Due to the large temperature difference between the CPCM modules and the entering cold HTF, the module temperature decreases quickly compared to other regions.

From a practical point of view, the large temperature swing occurred within the first and second configurations are not acceptable as it results in the nonuniform heating inside the heater and hence inadequate utilization of the latent heat of CPCM modules, whereas the third configuration exhibits relatively uniform temperature distribution and is considered to be the best option among all the CPCM arrangements studied in this work.

To quantitatively compare the performance of these three configurations, a parameter called heat storage efficiency, defined as the ratio of the stored heat during the charging process to the total supplied electrical power, is introduced:

$$\xi = \frac{Q_{CPCM} + Q_{insulation} + Q_{shell}}{P_s \cdot t} = 1 - \frac{\int_0^t f(T_{out})dt}{P \cdot t} \quad (1)$$

where Q_{CPCM}, $Q_{insulation}$, and Q_{shell} are respectively the heat stored by the CPCM modules, the insulation layers and the shell. P_s is the supplied electrical power and t is the charging time. Figure 6 shows the variations of the heat stored in the CPCM modules and heat storage efficiency with time for the three configurations. It can be seen that both the Q_{CPCM} and ξ increase with time for the three cases. During the off-peak

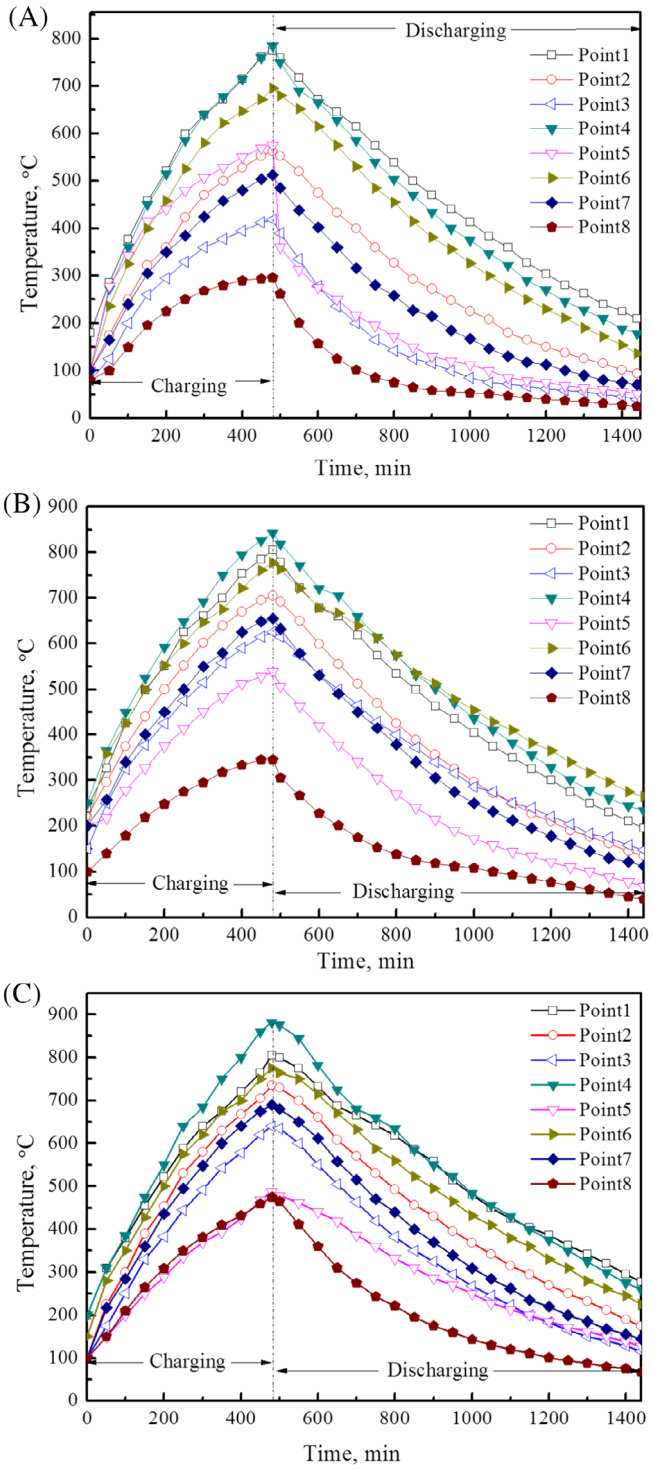

FIGURE 5 Time evolution of temperature distributions with the different CPCM module arrangements during charging and discharging. (A) case 1, (B) case 2, and (C) case 3

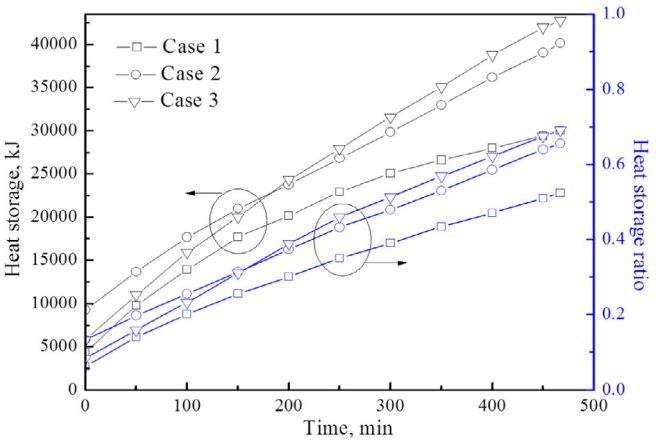

FIGURE 6 Heat stored and heat storage efficiency during charging with the three CPCM module arrangements

period, the Q_{CPCM} in the case 3 is the highest, which can be as high as ~42.5 MJ, followed by the case 2 at ~38.6 MJ and case 1 at ~29.8 MJ. The amount of heat stored within the heater corresponds to the heat storage efficiency for a given set of working conditions. The heat storage efficiency from high to low in turns are case 3 (~0.71), case 2 (~0.66) and case 1 (~0.54), as shown in Figure 6. The reason for this is that the thermal energy provided by the heating elements during the charging process has been transferred to the CPCM modules and the HTF, and the energy storage inside the heater is finally achieved through the modules in the forms of latent and sensible heat. The average temperature of the CPCM in the third configuration is the highest and hence stores the highest amount of heat. This in turn leads to the highest heat storage efficiency among the three configurations. On the contrary, the temperature distribution within the first configuration shows the most significant variation and the average temperature is the lowest, which results in only a small portion of phase change of the CPCM and hence, the lowest amount of heat stored and storage efficiency.

3.2 | Effects of CPCM module arrangements on the thermal cycle performance

Figure 7 shows the transient temperature distributions inside the heater for 10 consecutive days. For all the three cases, the heating power and airflow rate are kept the same, which are respectively ~2.4 kW and ~0.01 m/s. One can see that the first and second configurations show an undesirable large variation in the temperature distributions and the heating process has not reached a stable condition even after an operation for 10 days, suggesting the insufficient heat storage and varied HTF outlet temperature. This is clearly shown by the average temperature variation of the CPCM modules, which results in the CPCM to store the sensible form of heat for a large part of storage period of 8 hours, as shown in Figure 7A,B. This can lead to undesirable rise in both the heater and the indoor temperatures. Figure 7 also

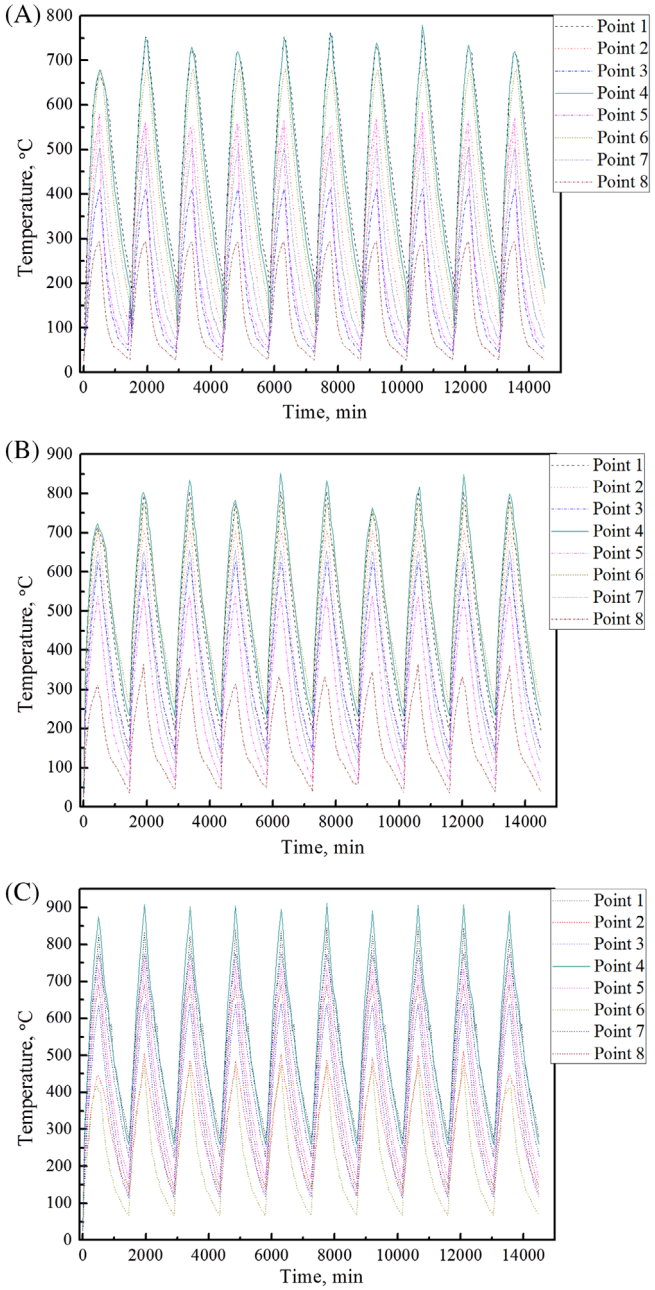

FIGURE 7 Transient behavior of the heater over the 10 consecutive days of operation at different CPCM arrangements. (A) case 1, (B) case 2, and (C) case 3

shows that the temperature variation inside the heater can be reduced significantly by using the third configuration. The maximum temperature variations in the first and second configurations during the 10 successive days of tests are respectively ~100°C and ~135°C, whereas the corresponding variation of the third configuration is only ~40°C, as shown in Figure 7C. During the first charging/discharging cycle, the maximum temperature in the third configuration is ~860°C since its initial temperature is the ambient temperature. From the second day, the temperature distributions

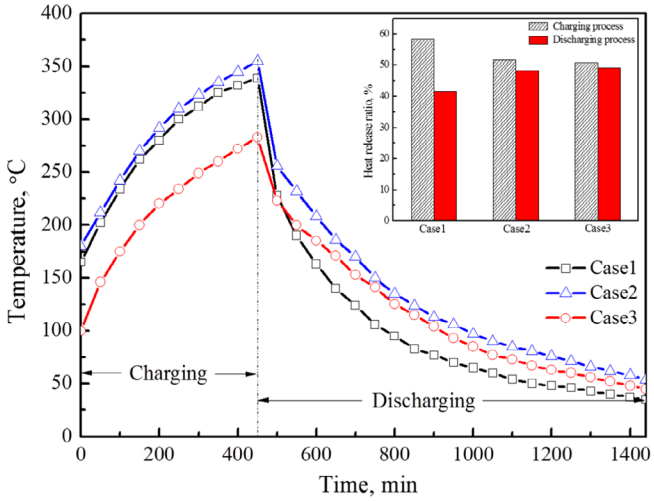

FIGURE 8 The outlet HTF temperature and the heat release ratio for different CPCM module arrangements

reach a periodic steady state with the maximum temperature at ~900°C. The slight fluctuation in the maximum temperature with the third configuration over the 10 days is likely due to the following two reasons. One is the increased ambient temperature, especially after the second day, and the other is the possibility of superheating due to incomplete discharge of the CPCM modules at the end of discharging process of each day.

3.3 | Effects of CPCM module arrangements on the HTF outlet temperature and room temperature

The time variation of the HTF outlet temperature for these three configurations is depicted in Figure 8. In all cases, the heat supplied is fixed at ~2.4 kW and the initial temperature of the CPCM modules is kept at ~100°C. One can see that the CPCM module arrangements have a great impact on the HTF outlet temperature of the heater. The second configuration gives the highest maximum outlet temperature of ~355°C, which is respectively ~15°C and ~72°C higher than that of the first and third configurations. Although the HTF temperature during charging with the third configuration is the lowest, it gives the most closest heat release ratio during a charging/discharging cycle; see the inset in Figure 8 where the heat release ratio is defined as the ratio of the heat released during charing to the total heat release of the heater:

$$\eta_{ch} = \frac{\int_0^{t_{ch}} f(T_{ch})dt}{\int_0^{t_{ch}} f(T_{ch})dt + \int_{t_{ch}}^{t_{dis}} f(T_{dis})dt} \tag{2}$$

$$\eta_{dis} = 1 - \eta_{ch} \tag{3}$$

where t_{ch} is the charging time; t_{dis} is the discharging time; T_{ch} is the outlet temperature during the charging process; T_{dis} is the outlet temperature during the discharging process. The above equations indicate that the area under the curves represents the heat released from the heater, as illustrated in Figure 8. One can see that, first, the heat release ratio during the charging process is the highest in case 1, whereas that in case 3 is the lowest. Second, the first configuration shows the largest heat release ratio variation during a charging/discharging cycle compared to other two configurations. Third, the third configuration gives the closest heat release ratio among the three configurations. The main reasons for these observations lie in the arrangement of the CPCM modules and the locations of HTF flow passage. During charge, the CPCM modules are mainly heated through radiation by the heating elements. When flowing in and the cold HTF first absorbs the heat from the CPCM modules located at the entrance, followed by heat transfer with the heating elements and CPCM modules in other regions. Due to natural convection, hot air rises, leading to the temperature of CPCM modules at the bottom region lower than that at the top region. Thus, the heated HTF will transfer the heat to the bottom CPCM modules before going out, leading to a reduced temperature decreases during process. As a result, before the bottom region modules are fully charged, the temperature of HTF at the outlet is always lower than that of CPCM at the bottom region. During discharge, the heating power is switched off and the heat released is through force convection from the modules to the HTF. Among the three cases, the interlaced arrangement of the CPCM modules in the third case gives the longest residence time of the HTF in the heater and hence the largest heat transfer area between the HTF and the modules for a given HTF velocity. Thus, the highest heat transfer rate could be achieved inside the heater, leading to the most heat stored/released during charging/discharging.

Figure 9 shows the time evolutions of the room temperature for the three different CPCM arrangements during a charging/discharging cycle. The room area is ~16.56 m^2 for case 1, ~20.16 m^2 for case 2, and ~20 m^2 for case 3. The power of the three cases is set as ~2.4 kW, for charging 8 hours from 10 PM to 6 AM. This provides a total heat of ~19.2 kWh, which should be sufficient to provide reasonably uniform heating over the whole day and keep the room temperature above ~18°C. One can see, however, that the room temperature of the case 1 shows a significant variation with the temperature varying between ~13.8°C and ~18.1°C. Such a large temperature swing is not acceptable. With the second configuration, the temperature variation is still high, although the room temperature can be maintained in the desired range for most of the time. The use of the third configuration can reduce the temperature swing and enhance the

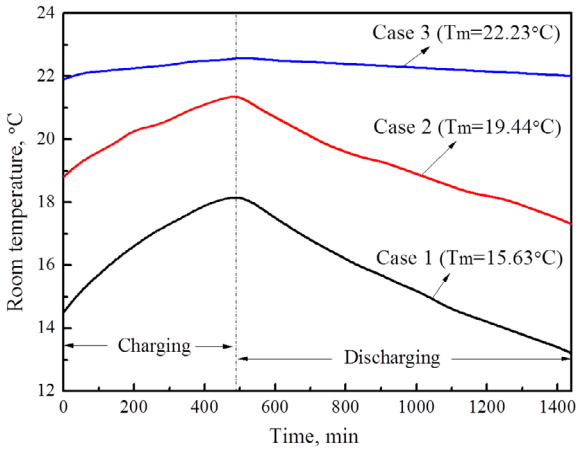

FIGURE 9 Variations of the room temperature with time for different CPCM module arrangements during a charging/discharging cycle

room thermal comfort level as illustrated in Figure 9, which shows that the room temperature varies between ~21.7°C and ~22.5°C over a day. Comparing the results illustrated in Figures 5 and 9, one could conclude that large variations in the room temperature are often accompanied by a large temperature variation inside the heater. Therefore, one needs to avoid such a variation to achieve uniform heating and efficient utilization of the latent heat storage of the CPCM modules.

4 | MATHEMATICAL MODEL FOR THE ELECTRICAL STORAGE HEATER

Due to the limitation and long period of the experimental procedure, it is difficult to monitor the temperature evolution of every point and moment, and evaluate the heater performance under every desired condition. Therefore, this section presents a complementary numerical study using a mathematical model that describes the transient heat transfer behaviour of the heater. The data form the modeling can be used to assess the performance of the heater. The third configuration with the interlaced arrangement of the CPCM modules is selected for the modelling, which has been demonstrated to be the optimal case studied in this work. The mathematical model is first validated with experimental data, followed by further modeling to compare the storage heater filled with CPCM and that of ferric oxide (FO) modules. The modelling results are also used to develop a temperature control strategy for the heater.

4.1 | Physical model and numerical modeling

Shown in Figure 10A is the schematic diagram of the computational model for the electrical storage heater, where the outer

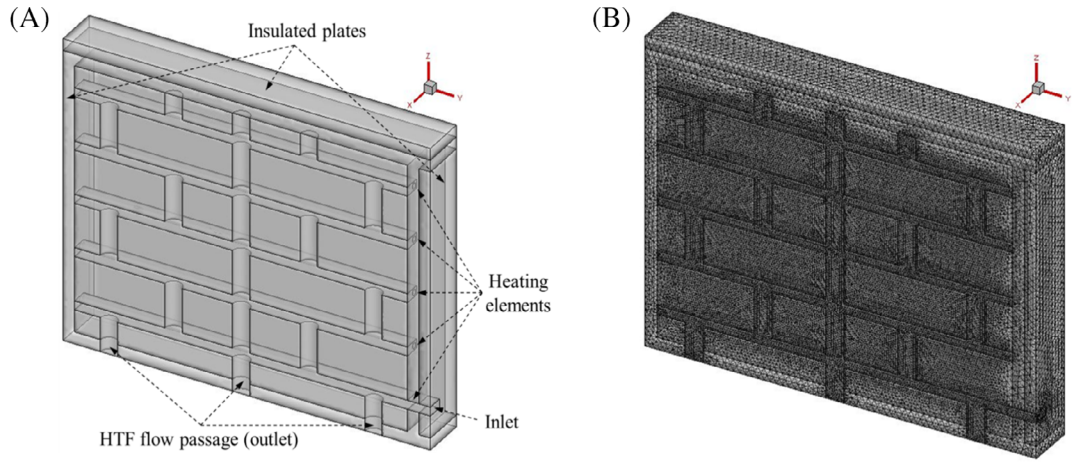

FIGURE 10 The physical model (A) and computational mesh (B) of the electrical storage heater

steel shell is not considered for simplification of the model. Due to the symmetry of the computational domain, only half of the geometry is modelled. The dimensions of the heater used in the modelling are the same as the experimental work for relevance, and the thermoproperties of storage and insulation materials used in the modelling can be found in the previous section.

The enthalpy-porosity approach is employed to model the phase transition process in the heater. For further simplifying the mathematic model, the following assumptions are made:

1. The volume change of the CPCM module during phase transition is neglected due to the stabilization of the structure.[27,28]
2. The CPCM module is considered as homogeneous and isotropic.
3. The heating element and CPCM module surfaces are treated gray and diffusive with emissivity and absorptivity independent of the wavelength. According to Kirchoff's law,[29] the emissivity is assumed to be equal to the absorptivity.
4. The HTF is regarded as transparent and its thermal radiation is not taken into consideration.[28,29]

According to the above assumptions, a three-dimension numerical model is established with the phase transition of the CPCM modules coupled with HTF heat transfer inside the heater. The governing equations including continuity, momentum, and energy equations for both the HTF and CPCM are given as follows.

For the HTF:

Continuity equation:

$$\frac{\partial \rho_{HTF}}{\partial t} + \nabla \cdot \left(\rho_{HTF} \vec{V}\right) = 0 \tag{4}$$

Momentum equation:

$$\frac{\partial (\rho_{HTF} u_{HTF})}{\partial t} + \vec{V} \cdot \nabla (\rho_{HTF} u_{HTF}) = -\frac{\partial P_{HTF}}{\partial x} + \mu_{HTF} \nabla^2 u_{HTF} \tag{5}$$

$$\frac{\partial (\rho_{HTF} v_{HTF})}{\partial t} + \vec{V} \cdot \nabla (\rho_{HTF} v_{HTF}) = -\frac{\partial P_{HTF}}{\partial y} + \mu_{HTF} \nabla^2 v_{HTF} \tag{6}$$

$$\frac{\partial (\rho_{HTF} w_{HTF})}{\partial t} + \vec{V} \cdot \nabla (\rho_{HTF} w_{HTF}) = -\frac{\partial P_{HTF}}{\partial z} + \mu_{HTF} \nabla^2 w_{HTF} - (\rho_{HTF} - \rho_0) g \tag{7}$$

Energy equation:

$$\frac{\partial \left(\rho_{HTF} c_{p,HTF} T_{HTF}\right)}{\partial t} + \vec{V} \cdot \nabla \left(\rho_{HTF} c_{p,HTF} T_{HTF}\right) = \nabla^2 (k_{HTF} T_{HTF}) \tag{8}$$

where u, v, and w stand for the HTF velocities along the x, y, and z axes, respectively. t is the time, P_{HTF} is the HTF pressure. μ_{HTF} is the HTF viscosity. ρ_{HTF} is the HTF density. ρ_0 is the reference density. $c_{p,\,HTF}$ and k_{HTF} are respectively the HTF heat capacity and thermal conductivity.

For the CPCM:

Based on the above assumptions, the energy equation of the entire CPCM region, where the thermal conduction is regarded as the dominant heat transfer mode, can be formulated as[27,28]:

$$\rho_C \frac{\partial H}{\partial t} = k_C \nabla^2 T_C + S_r \tag{9}$$

where ρ_C and k_C represent respectively the CPCM effective density and thermal conductivity. H is the specific enthalpy including the sensible enthalpy (h) and latent enthalpy (βL). β is the liquid fraction determined by the following Equation (10), which is zero in the entire solid PCM zones, one in the entire liquid zones, and between zero and one in the mushy phase zones.

$$\beta = \begin{cases} 0 \; if \; T_C \le T_s \\ \dfrac{T_C - T_s}{T_l - T_s} \; if \; T_s \le T_C \le T_l \\ 1 \; if \; T_C \ge T_l \end{cases} \tag{10}$$

The S_r in the Equation (9) is an energy source related to the thermal radiation. In this work, the surface-to-surface (S2S) based radiation model[28,29] is adopted to estimate the radiation in the heater with HTF assumed to be transparent. Given a surface i, the leaving heat flux consisted of two parts, directly emitted heat and reflected heat. The reflected heat flux is associated with the incident heat flux coming from the surroundings, and can be expressed in terms of leaving heat flux from all other surfaces. The leaving heat flux from the surface i can be written as:

$$q_{out,i} = \delta_i \sigma T_i^4 + \varphi_i q_{in,i} \tag{11}$$

where δ_i and φ_i stand for the emissivity and the reflectivity, respectively. σ is the Stefan-Boltzmann constant, T is the temperature, and $q_{in,\,i}$ is the incident heat flux on the surface i coming from other surfaces.

The incident heat flux on a surface, i, from another surface, j, is related to the S2S view factor, Ψ_{ji}. This factor is the ratio of heat flux leaving surface j that is incident on surface i. The incident heat flux, $q_{in,\,i}$, can be expressed by the heat flux leaving all other surfaces as:

$$A_i q_{in,i} = \sum_{j=1}^{M} A_j q_{out,j} \Psi_{ji} \tag{12}$$

where A_i is the surface area of i. For multiple surfaces, M, the following relationship can be used:

$$A_j \Psi_{ji} = A_i \Psi_{ij}, for \, j = 1,2,3,\ldots\ldots M \tag{13}$$

Combining Equations (13) and (12) yields:

$$q_{in,i} = \sum_{j=1}^{M} \Psi_{ij} \; q_{out,\,j} \tag{14}$$

Using Equation (14), Equation (11) can be transformed to:

$$q_{out,i} = \delta_i \sigma T_k^4 + \varphi_i \sum_{j=1}^{M} \Psi_{ij} \; q_{out,\,j} \tag{15}$$

The Ψ_{ij} can be determined by:

$$\Psi_{ij} = \frac{1}{A_i} \int_{A_i} \int_{A_j} \frac{cos\theta_i \; cos\theta_j}{\pi r^2} \Phi_{ij} \; dA_i \; dA_j \tag{16}$$

where θ stands for the angle between the normal and the connecting center line of the two surfaces. r stands for the distance between the two radiation surfaces. Φ_{ij} can be determined by the visibility of dA_i to dA_j. Φ_{ij}=1 for the case of dA_j is seeable to dA_i and 0 otherwise. Solution to Equations (15) and (16) gives the radiation heat flux for each surface in the computational domain.

4.2 | Correlations of effective thermoproperties for the CPCM

As mentioned in Section 2, the CPCM is composed of three ingredients of a PCM, a TCEM and a CSM. A number of theoretical correlations have been developed to predict the effective properties of this composite.[23,30] One commonly used approach is to regard two of components as a new material, which is then mixed with the third component. Here, the PCM and TCEM mixture is treated as the new material that is embedded into the micro-porous structure of the third component (CSM). Therefore, the effective thermoproperties can be determined as the properties of new mixture material and CSM.

For the PCM and TCEM mixture, the effective specific heat capacity, c_m, and density, ρ_m, can be respectively determined by the volume average approach,[23,28] and the effective thermal conductivity, k_m, can be evaluated by the Maxwell model[23]:

$$\frac{k_m}{k_{PCM}} = \frac{k_{TCEM} + 2k_{PCM} - 2\varepsilon(k_{PCM} - k_{TCEM})}{k_{TCEM} + 2k_{PCM} + \varepsilon(k_{PCM} - k_{TCEM})} \tag{17}$$

where k_{PCM} and k_{TCEM} represent the PCM and TCEM thermal conductivity, respectively. ε represents the volume ratio of TCEM in the PCM and TCEM mixture.

The effective thermal conductivity of the CPCM can be calculated by using the Zehner-Schlunder's model[31,32]:

$$\frac{k_{CPCM}}{k_m}=1-\sqrt{1-\phi}+\frac{2\sqrt{(1-\phi)}}{1-cB}\left(\frac{(1-c)B}{(1-cB)^2}\ln\frac{1}{cB}-\frac{B+1}{2}-\frac{B-1}{1-cB}\right) \tag{18}$$

where $c = k_m/k_{CSM}$, k_{CSM} stands for the thermal conductivity of the CSM. B stands for the shape factor given by[32]:

$$\mathrm{B}=a\left(\frac{1-\phi}{\phi}\right)^d \tag{19}$$

where a represents a constant and d is an exponent. In the work, the following values are adopted: a=1.364 and d = 1.055.[32]

The effective density of the CPCM can be estimated by:

$$\rho_{CPCM}=(1-\alpha)\rho_{CSM}+\alpha\rho_m \tag{20}$$

The effective heat capacity of the CPCM can be determined by:

$$c_{CPCM}\ \rho_{CPCM}=(1-\alpha)c_{CSM}\ \rho_{CSM}+\alpha c_m\rho_m \tag{21}$$

where c_{CSM} and ρ_{CSM} stand for respectively the CSM heat capacity and density. α is the volume ratio of the CSM in the CPCM.

4.3 | Initial/boundary conditions and numerical procedure

The whole calculation domain is set at a zero velocity and a temperature of T_0 initially, which is the same as the experimental conditions:

$$T_{HTF}=T_{CPCM}=T_0, u_{HTF}=v_{HTF}=w_{HTF}=0\ (t=0) \tag{22}$$

At the inlet of the heater, the HTF velocity and temperature can be given as:

$$T_{HTF,in}=T_{HTF,exp}, u_{HTF,in}=w_{HTF,in}=0, v_{HTF,in}=v_{HTF,exp}\ (t>0) \tag{23}$$

At the outlet of the heater, fully developed outflow condition is considered, and the outlet temperature and HTF velocity can be given as:

$$\left.\frac{\partial T_{HTF}}{\partial z}\right|_{out}=0, u_{HTF}=v_{HTF}=0, \left.\frac{\partial w_{HTF}}{\partial z}\right|_{out}=0\ (t>0) \tag{24}$$

At the interfaces between the HTF and CPCM modules, a coupled-wall boundary condition is used:

$$\mathrm{T}_{CPCM}|_{interface}=\mathrm{T}_{HTF}|_{interface} \tag{25}$$

Heat loss of the heater is taken into consideration although it is covered by two insulation layers. Thus, the boundary condition of the heater outer wall is given as:

$$-k_{HTF}\left.\frac{\partial T}{\partial n}\right|_{wall}=h_{wall}(T_{wall}-T_{ambient}) \tag{26}$$

where n is outer normal direction of the wall of the heater and $T_{ambient}$ is the ambient temperature.

All the numerical calculations are performed with the use of the commercial CFD software of ANSYS Fluent. A preprocessing software of Gambit is used for generating mesh. The finite volume approach is adopted for the discretization of the governing equations. The pressure staggering option (PRESTO) and second order upwind schemes are respectively employed for solving the pressure correction equation, and the momentum and energy equations. The semi-implicit pressure-linked equation (SIMPLE) algorithm is conducted to solve the coupling between the pressure and velocity. The user define function (UDF) code is used and interpreted to monitor the temperature and give feedbacks for manipulating the heat element inside the heater. Convergence is ensured for each time step with the criterions being respectively set as 10^{-4}, 10^{-5}, and 10^{-7} for the continuity, momentum, and energy equations.

5 | NUMERICAL RESULTS AND DISCUSSION

The numerical results and discussion are presented in this section with the grid independence validation being performed first, then the model validation and finally the extensive modelling on the comparison between the CPCM latent heat based heater and FO sensible heat based heater, as well as the temperature control strategy within the heater.

5.1 | Validation of numerical models

For the validation of the present numerical model, the grid sizes and time steps are checked prior to the comparison with the experimental results. In this work, the uniform unstructured grid with tetrahedral cells is adopted for mesh building as shown in Figure 10B. Four different grid sizes of 620 758, 1 050 460, 1 456 392, and 1 902 524 are tested and the results show that the cells of 1 456 392 is sufficient to ensure accuracy and reliability of the model without consuming additionally computational resources, and hence, is adopted for the subsequent simulations. Also, five different time steps of 0.01, 0.02, 0.05, 0.1, and 0.5 second are

compared and it has been demonstrated that 0.02 second is enough to achieve the required calculation precision.

The numerical results are compared with experimental data for model validation as illustrated in Figure 11, which plot the variations of temperature at point 6 and outlet as a function of the charging and discharging time. One can see that a good agreement between the experimental data and modelling results has been achieved with the maximum deviation (defined as $\nabla T/(T_{in} - T_{initial}) \times 100\%$) less than 10% and 12%, respectively for charging and discharging processes. These results give our confidence in the model. The deviation is likely associated with the nonuniform distribution of the HTF flow cross all the modules, which is considered in the modelling. The other reasons may be due to the prediction model for the effective thermal conductivity of the PCM and TCEM mixture. The theoretical Maxwell model present a lower prediction result than the actual value as it is accurate for noninteracting spherical particles.[30] But in this work, the used TCEM in the CPCM is flake shaped. In addition, the anisotropy influence on the effective thermal conductivity induced by flake shaped graphite is not considered in the theoretical model, which could also introduce the calculation errors. Besides that, the nonuniform distribution of ingredients and heterogeneity within the composite may also result in the deviation. Although every care has been taken to ensure good during the module fabrication, perfect mixing of ingredients at the CPCMs module level remains an engineering challenge.[4] Such non-homogeneous distribution of ingredients inside the composite also brings about the deviation between the modeling and experiments.

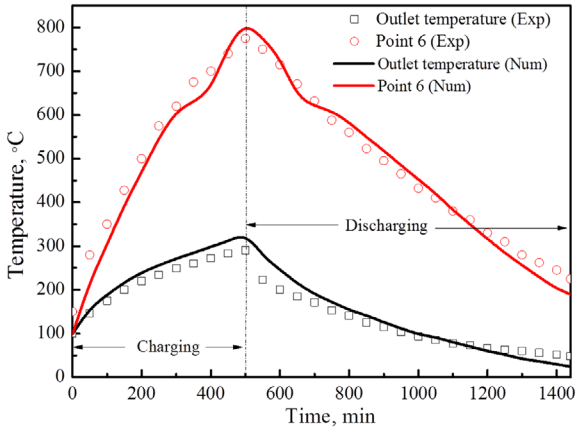

FIGURE 11 Comparison between experimental data and modeling results for thermocouple 6 and the outlet temperature as shown in Figure 3B

5.2 | Comparison between the CPCM based heater and FO based heater

To illustrate the advantage of the CPCM based electrical storage heater studied in this work, a comparison with the sensible heat storage heater is carried out. The commonly used FO is used for the comparison. The structural dimensions and their arrangements inside the heater as well as the modeling codes for the FO are the same as those for the CPCM. The thermoproperties of the FO can be found elsewhere.[28] Figure 12 shows the comparison of the total heat stored for the two heaters over the off-peak charging period. One can see that, for the CPCM based heater, the heat storage involves two main contributions with one coming from the sensible heat due to the temperature increase and the other the latent heat due to the phase change. At the beginning of charge, the heat stored is mainly in the sensible form and the process lasts around ~5 hours. After that, the CPCM module temperature increases to above the PCM melting point when the latent heat storage occurs. During the charging period, the sensible, latent and total heat storage within the CPCM based heater are respectively ~40 376.45, ~6241.16, and ~46 617.61 kJ. For the FO based heater, however, only sensible heat storage period is seen because of the lack of phase transition process. The total storage heat increases linearly with time and reaches ~46 406.82 kJ at the end of the charging process. These observations clearly indicates the advantages of the CPCM based electrical storage heater: for a given storage volume, the same power rating and the same amount of stored heat, the mass of the FO based electrical storage heater exceeds ~1.6 times than that of the CPCM based storage heater.

The comparison of the average module temperature and HTF outlet temperature between these two different heaters is presented in Figure 13. It can be seen that both the average module temperature and HTF outlet temperature of the heater with CPCM are higher than that of the heater with FO over the entire charging process. This is because of the high thermal conductivity of the composite PCM modules. Due to the containment of the CSM and TCEM, the effective thermal conductivity of the CPCM is largely improved, leading to a higher heat transfer rate and hence a higher temperature in the CPCM based storage heater in comparison with the FO based storage heater. Based on temperature difference between the two heaters with different materials, it can be concluded that for the same mass and the same power rating, the heat storage capacity of the CPCM based electrical storage heater can be nearly ~68% higher than that of the FO based heater.

5.3 | Temperature control strategy within the heater

As discussed in Section 3, although the interlaced arrangement of the CPCM modules within the heater offers the best performance in terms of heat storage ratio and

charging/discharging efficiency, the maximum temperature of the CPCM modules during the charging process can reach ~890°C, which exceeds the maximum allowable temperature of the carbonate salt based CPCM (~850°C), leading to undesirable decomposition of the CPCM in long-term applications. Therefore, in order to avoid the CPCM modules from being overheated and decomposed, a temperature control strategy is essential through which the maximum temperature inside the heater can be controlled by manipulating the start-stop of power of the heating elements. This means that, the heating elements will be switched off to stop the heating of the CPCM modules when the highest temperature of the modules exceeds a presetting safe value (the upper bound), where the heat transfer in the modules field is mainly dominated by the thermal conduction and convection with HTF. On the contrary, if the modules temperature falls below a lower presetting value (the lower bound), the power will be switched on to reheat the CPCM and to ensure the sufficient heat stored within the heater. For doing so, the upper and lower bounds are respectively set as ~750°C and ~650°C. Three monitoring points, *T1*, *T2* and *T3* at the middle upper region of the heater (Z = 405 mm) close to the heating elements, are selected for the investigation since the highest temperature inside the heater is found to be in this region (see Figure 4). *T1* is located at the surface of the HTF flow passage, and *T2* and *T3* are respectively 15 and 35 mm from the HTF flow passage, as illustrated in Figure 14.

Figure 15 shows the time evolution of the temperature at the monitor points and the heat flux of heating elements at the different control cases. One can see clear variations on the temperature and heat flux inside the heater. In the case of the point *T1* which is nearest to the heating element is selected as the control position, the maximum temperature and average temperature inside the heater are respectively ~700°C and ~655.3°C. Although both them are below the CPCM decomposition temperature, the switch on and off times of heating elements exceeds eight times within a charging and discharging cycle. Such a frequent start-stop could shorten the heating element lifespan. When the point *T3* is used for temperature control, it presents the highest average temperature inside the heater and also only one start-stop operation is needed, but the maximum temperature reaches ~760°C, exceeding the upper bound. For the control position chosen to be ~15 mm away from the heating elements (the point *T2* illustrated in Figure 14), both the average temperature (~667.61°C) and maximum temperature (~721.2°C) within the heater can meet the requirements with two start-stops observed over the 8-hour charging period. Moreover, in such a case, the CPCM module average temperature is around ~12°C higher than that

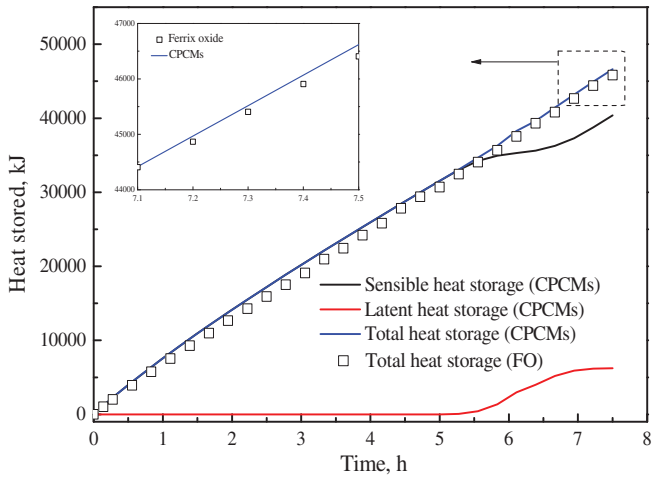

FIGURE 12 Comparison of the heat stored between the CPCM based electrical storage heater and FO based electrical storage heater over the charging period. CPCM, composite phase change material; FO, ferric oxide

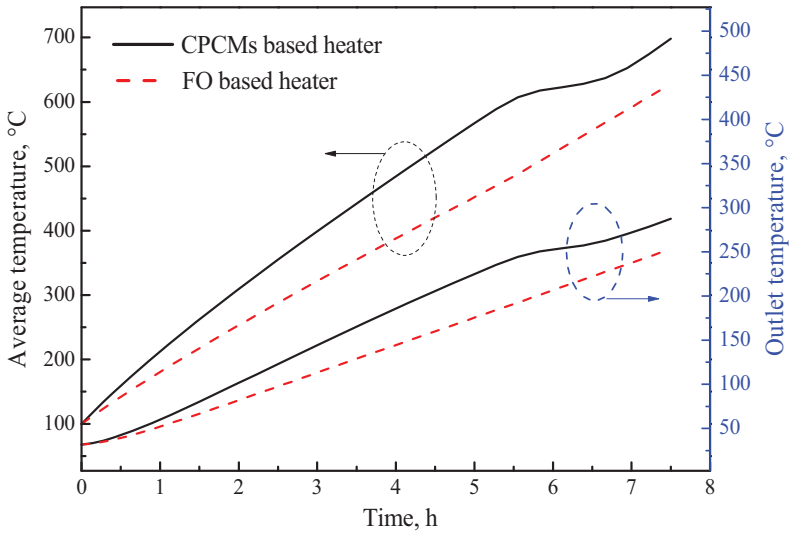

FIGURE 13 Comparison of the average temperature and outlet temperature between the CPCM based electrical storage heater and FO based electrical storage heater over the charging period. CPCM, composite phase change material; FO, ferric oxide

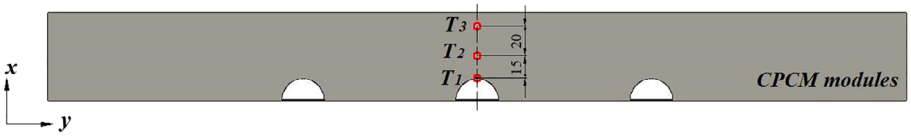

FIGURE 14 Schematic diagram of the monitoring points for temperature control within the heater

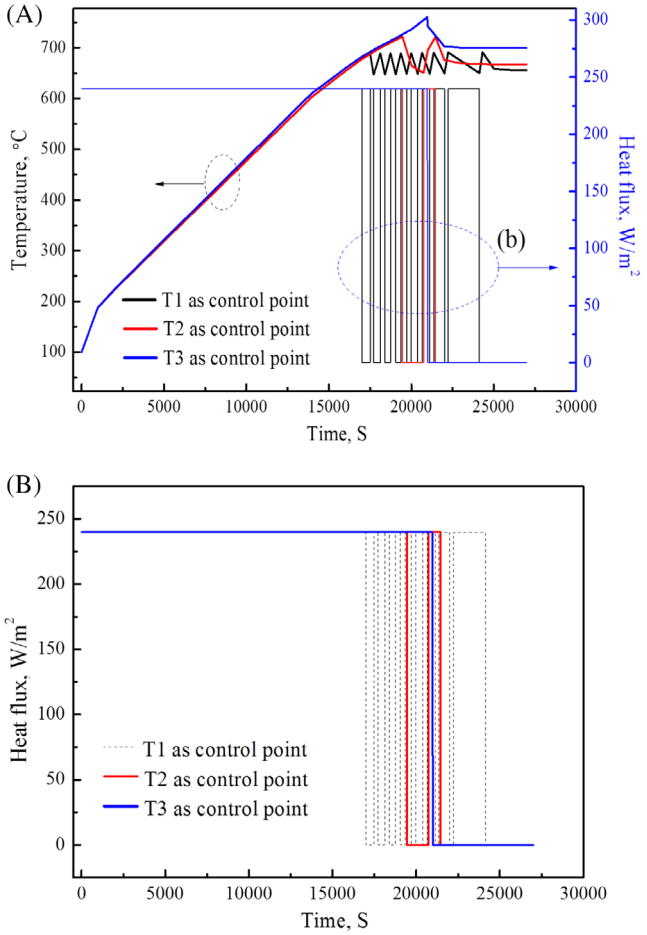

FIGURE 15 (A) Variations of the temperature at monitor points and heating flux of heating element at the case of different control point with time, and (B) the enlarged illustration indicated on the figure (A)

of the case of selection of *T1* as the control point, indicating more heat can be stored at the same charging duration. These observations suggest the importance of temperature monitor point selection and the enhancement of the heat storage performance within the electrical storage heater could be achieved by regulating the temperature control strategy.

6 | CONCLUSIONS

This work concerns a high temperature storage heater containing an inorganic salt based CPCM for electrical load shift and cost reduction. The storage heater consists of CPCM modules with embedded electrical elements for charging at off-peak hours and flow channels for discharging the stored heat in a controlled manner when needed. The flow channels are for HTF to exchange heat with the CPCM modules and transport the heat to the heating space. A series of experiments are carried out to study the charging and discharging behavior of the storage heater. The effects of the flow channel arrangements between the CPCM modules, and the heating element arrangements inside the heater are studied. A mathematical model is also developed to investigate the performance of the storage heater with a focus on performance comparison of the storage heater filled with the CPCM and that with the ferric oxide bricks, and evaluation of temperature control strategy for the CPCM based storage heater. The conclusions are summarized as follows:

1. The CPCM module arrangements have a significant influence on the storage heater performance in terms of the temperature distribution of the CPCM modules and HTF outlet temperature, and the heat storage and release efficiencies during both the charging and discharging processes. For a given working condition, the parallel arrangements of the CPCM modules present a large temperature swing and a nonuniform heating inside the heater, and hence inadequate utilization of the latent heat of CPCM modules, whereas the interlaced configuration exhibits relevantly uniformed temperature distribution and is showed the best option for CPCM modules arrangement.
2. The interlaced arrangement of CPCM modules inside the heater can effectively reduce the temperature swing and enhance the room thermal comfort level, demonstrating the heater operated for 8 hours during the off-peak period is sufficient to achieve reasonably uniform heating in which the room temperature keeps almost stable at temperatures varying between 21.7°C and 22.5°C over a day.
3. The CPCM based storage heater gives a superior performance than the ferric oxide based storage heater. Given the storage volume, the power rating, and the amount of stored heat, the mass of the ferric oxide based storage heater is more than 1.6 times that of the CPCM based storage heater. Given the mass and power rating, the heat storage capacity of the heater with CPCM is nearly 68% larger than that of the heater with ferric oxide.
4. The enhancement of the heat storage performance in the electrical storage heater could be achieved by regulating the

temperature control strategy. It is found that the average temperature and the maximum temperature inside the electrical storage heater could meet the safe and heat storage requirements if the temperature monitor position is selected to be ~15 mm away from the heating elements. In such a case, heating elements only needs two start-stops over the 8-hour charging period.

ACKNOWLEDGMENTS

The authors acknowledge the funding supports from the UK Engineering and Physical Sciences Research Council (EPSRC) under grants EP/P004709/1, EP/P003435/1, the British Council under 2016-RLWK7-10243 and 2018-RLWK10-10594.

NOMENCLATURE

SYMBOLS

a	constant value
B	shape factor
c_p	specific heat, (J/[kg·K])
g	gravitational acceleration, (m/s^2)
h	sensitive heat, (J)
H	enthalpy, (J)
k	thermal conductivity, (W/[m·K])
L	latent heat, (J/kg)
M	surface amount
m	mixture of PCM and TCEM
P	pressure, (Pa)
P_s	supplied electrical power, (kW)
q	heat flux (W/m^2)
Q	heat stored (kJ)
S_r	energy source term, (W/m^3)
t	time, (s)
T	temperature, (°C)
u, v, w	velocity in x, y, z direction, (m/s)
x, y, z	Cartesian coordinates

GREEK SYMBOLS

β	liquid fraction
ϵ	volume ratio of the TCEM in the PCM/TCEM mixture
ξ	heat storage ratio
δ	emissivity
η	heat release ratio
θ	angle, (°)
μ	viscosity, (kg/[m·s])
ρ	density, (kg/m^3)
σ	Stefan-Boltzmann constant
φ	reflectivity
Ψ	view factor

SUBSCRIPTS

ch	charging process
d	Exponent constant
dis	discharging process
in	inlet value
interface	interface between the CPCM and the HTF
i, *j*	surface number
l	liquid
s	solid
CPCM,*C*	composite phase change material
CSM	ceramic skeleton material
HTF, *f*	heat transfer fluid
PCM	phase change material
TCEM	thermal conductivity enhancement material

ORCID

Chuan Li https://orcid.org/0000-0003-4605-7072

REFERENCES

1. Heremans JP. Thermoelectricity: the ugly duckling. *Nature*. 2014; 508:327-328. https://doi.org/10.1038/508327a.
2. Wang ZY, Diao YH, Liang L, Zhao YH, Zhu TT, Bai FW. Experimental study on an integrated collector storage solar air heater based on flat micro-heat pipe arrays. *Energ Buildings*. 2017;152: 615-628. https://doi.org/10.1016/j.enbuild.2017.07.069.
3. World Health Organization (WHO). Residential heating with wood and coal: health impacts and policy options in Europe and North America. 2015, ISBN: 978 92 890 50760.
4. Patteeuw D, Bruninx K, Arteconi A, Delarue E, Dhaeseleer W, Helsen L. Integrated modelling of active demand response with electric heating systems coupled to thermal energy storage systems. *Appl Energy*. 2015;151:306-319. https://doi.org/10.1016/j.apenergy.2015.04.014.
5. Wang Z, Diao Y, Zhao Y, Liang L, Wang T. Experimental study on the new type of electrical storage heater based on flat micro-heat pipe arrays. *Sci China Technol Sci*. 2018;61:219-231. https://doi.org/10.1007/s11431-017-9121-6.
6. Darby SJ. Smart electric storage heating and potential for residential demand response. *Energ Effic*. 2018;11:67-77. https://doi.org/10.1007/s12053-017-9550-3.
7. Lin K, Zhang Y, Xu X, Di H, Yang R, Qin P. Modeling and simulation of under-floor electric heating system with shape-stabilized PCM plates. *Build Environ*. 2004;39:1427-1434. https://doi.org/10.1016/j.buildenv.2004.04.005.
8. Lacroix M, Duong T. Experimental improvements of heat transfer in a latent heat thermal energy storage unit with embedded heat sources. *Energy Convers Manag*. 1998;39:703-716. https://doi.org/10.1016/S0196-8904(97)10011-5.
9. Brousseau P, Lacroix M. Study of the thermal performance of a multi-layer PCM storage unit. *Energy Convers Manag*. 1996;37: 599-609. https://doi.org/10.1016/0196-8904(95)00207-3.
10. Laouadi A, Lacroix M. Thermal performance of a latent heat energy storage ventilated panel for electric load management. *Int J*

Heat Mass Transf. 1999;42:275-286. https://doi.org/10.1016/S0017-9310(98)00121-5.

11. Li C, Li Q, Cong L, et al. MgO based composite phase change materials for thermal energy storage: the effects of MgO particle density and size on microstructure characteristics and thermoproperties. *Appl Energy*. 2019;250:81-91. https://doi.org/10.1016/j.apenergy.2019.04.094.
12. Li C, Li Q, Cong L, et al. Carbonate salt based composite phase change materials for medium and high temperature thermal energy storage: a microstructural study. *Sol Energ Mat Sol C*. 2019;196:25-35. https://doi.org/10.1016/j.solmat.2019.03.035.
13. Li M, Mu B. Effect of different dimensional carbon materials on the properties and application of phase change materials: a review. *Appl Energy*. 2019;242:695-715. https://doi.org/10.1016/j.apenergy.2019.03.085.
14. Farid MM, Chen XD. Domestic electrical space heating with heat storage. *J Power Energy*. 1999;213:83-92. https://doi.org/10.1243/0957650991537455.
15. Farid MM, Kong WJ. Underfloor heating with latent heat storage. *J Power Energy*. 2001;215:601-609. https://doi.org/10.1243/0957650011538839.
16. Wang X, Liu J, Zhang Y, Di H, Jiang Y. Experimental research on a kind of novel high temperature phase change storage heater. *Energy Convers Manag*. 2006;47:2211-2222. https://doi.org/10.1016/j.enconman.2005.12.004.
17. Li C, Li Q, Li Y, et al. Heat transfer of composite phase change material modules containing a eutectic carbonate salt for medium and high temperature thermal energy storage applications. *Appl Energy*. 2019;238:1074-1083. https://doi.org/10.1016/j.apenergy.2019.01.184.
18. Li C, Li Q, Ding Y. Investigation on the effective thermal conductivity of carbonate salt based composite phase change materials for medium and high temperature thermal energy storage. *Energy*. 2019;176:728-741. https://doi.org/10.1016/j.energy.2019.04.029.
19. Ge Z, Li Y, Li D, et al. Thermal energy storage: challenges and the role of particle technology. *Particuology*. 2014;15:2-8. https://doi.org/10.1016/j.partic.2014.03.003.
20. Ge Z, Ye F, Ding Y. Composite materials for thermal energy storage: enhancing performance through microstructures. *ChemSusChem*. 2014;7:1318-1325. https://doi.org/10.1002/cssc.201300878.
21. Ge Z, Ye F, Cao H, Leng G, Qin Y, Ding Y. Carbonate-salt-based composite materials for medium and high temperature thermal energy storage. *Particuology*. 2014;15:77-81. https://doi.org/10.1016/j.partic.2013.09.002.
22. Li C, Li Q, Cao H, et al. Wettability of eutectic NaLiCO3 salt on magnesium oxide substrates at 778 K. *Appl Surf Sci*. 2018;442:148-155. https://doi.org/10.1016/j.apsusc.2018.02.082.
23. Zhao B, Li C, Jin Y, et al. Heat transfer performance of thermal energy storage components containing composite phase change materials. *IET Renew Power Gene*. 2016;10:1515-1522. https://doi.org/10.1049/iet-rpg.2016.0026.
24. Lin K, Zhang Y, Xu X, Di H, Yang R, Qin P. Experimental study of under-floor electric heating system with shape-stabilized PCM plates. *Energ Buildings*. 2005;37:215-220. https://doi.org/10.1016/j.enbuild.2004.06.017.
25. Lin K, Zhang Y, Di H, Yang R. Study of an electrical heating system with ductless air supply and shape-stabilized PCM for thermal storage. *Energy Convers Manag*. 2007;48:2016-2024. https://doi.org/10.1016/j.enconman.2007.01.014.
26. Zhou G, Zhang Y, Zhang Q, Lin K, Di H. Performance of a hybrid heating system with thermal storage using shape-stabilized phase-change material plates. *Appl Energy*. 2007;84:1068-1077. https://doi.org/10.1016/j.apenergy.2006.09.015.
27. Li C, Li Q, Ding Y. Carbonate salt based composite phase change materials for thermal energy storage: from component to device level performance through modelling. *Renew Energy*. 2019;140:140-151. https://doi.org/10.1016/j.renene.2019.03.005.
28. Li C, Li Q, Ding Y. Investigation on the thermal performance of a high temperature packed bed thermal energy storage system containing carbonate salt based composite phase change materials. *Appl Energy*. 2019;247:374-388. https://doi.org/10.1016/j.apenergy.2019.04.031.
29. Ma F, Zhang P. Investigation on the performance of a high-temperature packed bed latent heat thermal energy storage system using Al-Sl alloy. *Energy Convers Manag*. 2017;150:500-514. https://doi.org/10.1016/j.enconman.2017.08.040.
30. Wang M, Pan N. Predications of effective physical properties of complex multiphase materials. *Mater Sci Eng R Rep*. 2008;63:1-30. https://doi.org/10.1016/j.mser.2008.07.001.
31. Chan KC, Chao CYH. A theoretical model on the effective stagnant thermal conductivity of an adsorbent embedded with a highly thermal conductive material. *Int J Heat Mass Transf*. 2013;65:863-872. https://doi.org/10.1016/j.ijheatmasstransfer.2013.06.071.
32. Hsu CT, Cheng P, Wong KW. Modified Zehner-Schlunder models for stagnant thermal conductivity of porous media. *Int J Heat Mass Transf*. 1994;37:2751-2759. https://doi.org/10.1016/0017-9310(94)90392-1.

How to cite this article: Li C, Li Q, Zhao Y, et al. A novel high temperature electrical storage heater using an inorganic salt based composite phase change material. *Energy Storage*. 2019;1:e88. https://doi.org/10.1002/est2.88